Response Surface Estimation of Trim Controls for a Compound Helicopter with Control Redundancy

Jean-Paul Reddinger
Ph.D. Student
Rensselaer Polytechnic Institute
Troy, NY

Farhan Gandhi
Professor
Rensselaer Polytechnic Institute
Troy, NY

ABSTRACT

For a compound helicopter with sufficient control redundancy, this study presents a knowledge based method for estimating the set of controls required to maintain trim as a function of additional controls (main rotor RPM, auxiliary thrust, and stabilator pitch). Trim analyses with parametric sweeps through the additional controls are simulated in RCAS for a compound helicopter model based on a UH-60A. The resulting data sets are used to construct quadratic regression fit models, which represent the response of the six classical trim controls subject to variation in additional controls. In hover these models predict states that aren't fully trimmed, but the force and moment residuals are low. At forward flight speeds the response of the controls are no longer quadratic, and these force and moment residuals increase. Eliminating outlier trim states from the training data set gives the greatest improvement to the predictive capabilities of the model, but sacrifices some of the range of controls over which the model can apply. Kriging interpolation retains the full range of controls, but produces multiple local minima. For application to estimating the best controls for minimization of power it is shown that both truncating the data set and Kriging can provide good estimates of the minimum power trim state controls without excessive force and moment residuals. Allocating the additional controls as given by the response surfaces and solving for trim returned a slightly lower power than was found in the parametric trim sweeps.

NOTATION

A	quadratic coefficient matrix for regression fit model
B	linear coefficient vector for regression fit model
C	constant coefficient for regression fit model
P	total power
R	main rotor radius
T	collective thrust control of auxiliary propellers
V_∞	freestream velocity
W	vehicle gross weight
X	$m \times 1$ array of predictors
Y	$n \times 1$ array of response variables
a	speed of sound
d	2-norm distance between two sets of predictor-response pairs
m	number of response surface predictor variables
n	trim degrees of freedom
Δ_T	differential thrust control of auxiliary propellers
Ω	main rotor rotational speed
α	vehicle pitch attitude
δ_a	differential ailerons
δ_s	stabilator pitch angle
θ_0	collective pitch
θ_{1c}	longitudinal cyclic pitch
θ_{1s}	lateral cyclic pitch
ρ_∞	freestream air density
ϕ	vehicle roll attitude
$\hat{(\,)}$	quantity as predicted by response surfaces
$\oplus$	operator denoting a concatenation of two vectors

Presented at the AHS 72nd Annual Forum, West Palm Beach, Florida, May 17–19, 2016.

INTRODUCTION

Conventional rotary-wing aircraft are usually capable of maximum speeds no greater than 150–170 kts, limited by the onset of advancing blade compressibility, retreating blade stall, high vibration, and deterioration in rotor performance leading to an eventual inability to produce the forces and moments required to equilibrate the aircraft. One approach to overcome these challenges is to tilt the rotor forward to function as an axial propeller, while transferring the lifting function to wings in forward flight. Tilt-rotor aircraft like the Bell-Boeing V22-Osprey are thereby capable of attaining maximum speeds greater than 275 kts, but have a significantly higher empty-weight fraction, increased complexity, and reduced hover and low-speed performance (Ref. 1). If the maximum speed requirement is in the 200–250 kt range, a lift-offset coaxial configuration with auxiliary propulsion, or a slowed-rotor compound configuration with auxiliary lift and propulsion may be more viable solutions, offering reduced complexity and improved hover performance relative to a tilt-rotor aircraft. Coaxial rotor technology, using two counter-rotating rotors with each generating lift on its advancing side in the high-speed regime, was referred to as the Advancing

Blade Concept and first implemented on the Sikorsky XH-59 helicopter in the 1970's (Ref. 2). After a hiatus of several years, Sikorsky Aircraft Corp. developed a second generation high-speed coaxial rotor aircraft prototype, the X2 Technology Demonstrator (Refs. 3–6), which improved on many of the shortcomings of the XH-59. These technologies are also being scaled up by Sikorsky for application to the S-97 Raider, and jointly by Sikorsky and Boeing for the SB>1 Defiant in response to the Armys Joint Multi-Role program (Refs. 7, 8).

While lift-offset coaxial configurations generate lift on the advancing side of each rotor, a slowed-rotor compound helicopter uses a fixed wing to provide the majority of the aircraft lift in high speeds. Efforts focused on the development of slowed rotor compound configurations go back several decades, with the AH-56 Cheyenne compound helicopter (Ref. 9) representing a significant milestone in the 1960's, but because of complications in the development and testing phase, the program was cancelled. More recently, the Large Civil Tandem Compound (LCTC) was one of the concepts considered under the NASA Joint Heavy Lift Program (Ref. 10). Piasecki Aircraft Corp. modified an SH-60 Sea Hawk with a lifting wing and the company's Vectored Thrust Ducted Propeller (VTDP) to operate at speeds greater than 170 kts (Ref. 11). Airbus Helicopter's X^3 compounded the AS 365 Dauphin with propellers mounted on wings for auxiliary lift and propulsion at high speed (Ref. 12). It has since set the current speed record of 255 kts for an edgewise rotor in level flight.

In addition to the major design and development programs discussed above, many fundamental studies over the years have focused on the performance and benefits of compound helicopters (Refs. 13–23). To contribute to understanding of the aeromechanical behavior of slowed-rotors in high speed flight, a series of wind tunnel experiments were conducted on UH-60A rotors at high advance ratios under the NASA/Army UH-60A Airloads Program (Ref. 24).

Supplementing the classical helicopter controls with control of the rotor RPM, wing flaps and ailerons, elevators, and auxiliary thrust, provides an opportunity for compound helicopters to exploit control redundancy and fly the aircraft in any number of different ways. For example, the controls could be selected to minimize the power requirement, vibrations, blade flapping, acoustic noise, or some weighted combination thereof, while satisfying vehicle force and moment equilibrium in steady level flight (Refs. 25–31), or to improve handling qualities in maneuvering flight (Ref. 32). In a recent effort, Horn and co-workers (Refs. 33, 34) attempted to determine the optimal control configurations of a high-speed compound aircraft in-flight, using Fly-to-Optimal methods. The approach, based on perturbation of individual controls, requires a substantial amount of time, especially when multiple redundant controls are used, and the solution is itself dependent on the sequence of control perturbations. The Fly-to-Optimal approach makes no use of any prior knowledge of the system in attempting to determine the best compound helicopter controls.

This study introduces a novel method of estimating the controls required to maintain trim for a compound helicopter at any flight speed. It compares several methods of producing response surfaces which can be used to predict trim controls to varying degrees of success under different conditions. The response surfaces are then used to determine the set of controls which minimize a power in steady level flight.

COMPOUND HELICOPTER MODELING AND ANALYSIS

The compound helicopter model used in the simulations of this study is adapted from a UH-60A rotor and fuselage model, and is very similar to the model used in Ref. 30. Table 1 provides a summary of the compound configuration's major subsystems and their characteristics. The configuration is designed for high speed flight, and the model used is representative of that. Auxiliary propulsion is used to provide thrust in high-speed flight, so the forward shaft tilt present on the UH-60A is removed. Furthermore, the UH-60A twist provides excellent hover performance, but the large non-linear twist rate results in high negative lift and drag at the advancing blade tips for high advance ratios. A more moderate $-8°$ twist will be considered in this study. Other features of the UH-60A rotor including airfoil selections, chord distribution, and sectional mass and stiffness properties are left unchanged. The airfoil aerodynamic coefficients are interpolated from non-linear lookup tables.

Table 1. Compound helicopter configuration

Characteristic	Measurement
Gross Weight	20,110 lbs
C.G. Location	1.5 ft aft, 5.8 ft below hub
Main Rotor	
Rotor Radius	26.8 ft
Nominal Rotor Speed	258 RPM
Nominal Blade Twist	$-8°$
Shaft Tilt	$0°$
Airfoils	SC-1094 R8/SC-1095
Horizontal Stabilizer	
Effective Area	43 ft^2
Airfoil	NACA 0012
Wing	
Planform Area	220 ft^2
Chord	5 ft
Wingspan	44 ft
Incidence Angle	$3.8°$
Aerodynamic Properties	Aerostar FJ-100
C.P. Location	0.5 ft aft, 6.5 ft below hub
Auxiliary Propellers	
Radii	4.5 ft
Speed	1,934 RPM
Solidity	0.12
Locations	10 ft laterally, on each wing

The gross takeoff weight is increased to 20,110 lbs, which is equivalent to the takeoff weight of the Piasecki X-49A

SpeedHawk. This increased weight can be assumed to include the weight of the wings, auxiliary propulsion, and any additional weight required to compound the UH-60A airframe. To model fuselage drag, the compounded fuselage is assumed to be more streamlined than the UH-60A fuselage. A UH-60A has a minimum equivalent flat plate drag area of 35.14 ft^2 (Ref. 35). According to trends established by Ormiston (Ref. 19), a modern aircraft at this gross weight that is designed for high speed flight can be expected to have an equivalent flat plate drag area of 18.49 ft^2. The quadratic relation between vehicle pitch attitude and drag as measured for the UH-60A was maintained, resulting in the following expression for the equivalent flat plate drag area as a function of vehicle pitch (in degrees).

$$f_D = 18.487 + 0.0441\alpha^2 \ (\text{ft}^2)$$

The wing model is based on the three dimensional lift, drag, and moment coefficients for the wing of the Aerostar FJ-100, which is the wing used on the X-49A. For the purpose of the study in in Ref. 30, it has been set at an incidence of 3.8°, so that for pitch-level flight at 225 kts it will be flying close its peak L/D of 22.4, and scaled in area from 178.2 ft^2 to 220 ft^2 so that at this attitude it will be lifting about 83% of the gross weight of the aircraft. With only 1.2° of nose-up vehicle pitch, the wings can produce enough aerodynamic lift to completely offset the aircraft weight, and will still be operating at an L/D of 21.2. Interference between the wing and rotor is not modeled in this study. In a similar study by Moodie and Yeo, interference effects were shown to increase the total power by less than 1% (Ref. 21). Aileron deflections are modeled as a roll moment applied at the root of the wings. This model is representative of differential aileron deflection, which produces negligible adverse yaw. Increased drag due to aileron deflection is not modeled.

The auxiliary thrust is modeled as a point force (parallel to the waterline of the aircraft) and a yaw moment (parallel to the rotor torque vector), which are vertically applied in line with the center of gravity, and longitudinally between the quarter-chord of the wings. This is done so that increased total auxiliary thrust acts solely on longitudinal force does not produce a coupled pitching moment. The magnitude of the thrust and the yaw moment are directly prescribed as controls. Propeller power is determined using a blade element vortex theory (BEVT) model of two pitch controlled four-bladed propellers with a 4.5 ft radius at 1,934 RPM.

The horizontal stabilizer is modeled after the size and location of the UH-60A stabilizer, with airfoil coefficients interpolated from a table of NACA 0012 wind tunnel data. Interference between the wake of the rotor and the horizontal tail is ignored.

To simulate the inflow in hover, a 12×12 dynamic inflow model is implemented. Interference effects between the rotor, fuselage, and wings are not modeled. A dual core prescribed wake model is selected to model the inflow in forward flight, which captures the effects of producing negative lift on the advancing tip of the blade.

The simulations are produced using the US Army's Rotorcraft Comprehensive Analysis System (RCAS) (Ref. 36). The structural and aerodynamic models are built to the above mentioned specifications in RCAS using 13 elastic beam elements, 36 aerodynamic sections, and an azimuthal resolution of 5° for calculation of airloads. The flap and lag hinges, and pitch bearings are modeled as torsional spring/damper elements, and pitch control is prescribed through a spring element with a stiffness that is representative of the pitch link and swashplate stiffness of a UH-60A. As a computational tool, RCAS has been independently validated against wind tunnel data of an untwisted H-34 rotor at advance ratios up to 0.46 using a prescribed wake model (Ref. 37).

RESPONSE SURFACE METHOD

The presentation of methodology in this section will be accompanied by a detailed set of results for a hovering compound helicopter.

During any point when the helicopter is within some tolerance of fully trimmed flight, control settings and flight condition data can be taken. This data could include some of the following parameters.

$\theta_0 \quad \theta_{1c} \quad \theta_{1s} \quad \Delta_T \quad \alpha \quad \phi \quad \Omega \quad T \quad \delta_s \quad \delta_a$ (controls)

$V_\infty \quad \rho_\infty \quad W$ (flight conditions)

A large set of trim states are produced in RCAS for the hovering flight condition with constant air density and gross weight. These simulations will be used as training data for the model from which trim controls will be estimated. In practical application, this role can be replaced by actual flight data.

In hover, auxiliary thrust and variable main rotor speed provide two degrees of control redundancy. Stabilator pitch will be additionally introduced in a following section focusing on forward flight. The six conventional trim variables (collective pitch, lateral cyclic, longitudinal cyclic, pedal, pitch attitude, and roll attitude) are then solved for through the trim procedure to reduce total residual forces and moments to within 40 lbs and 40 lbs-ft. 105 trim states which satisfy the constraints in Table 2 are produced by sweeping auxiliary thrust from -3500 to 3500 lbs in 500 lbs increments, and rotor rotational speed from 21 to 27 rad/s in 1 rad/s increments (200 to 258 RPM). Such large values of auxiliary thrust can be expected to produce unnecessarily high blade flapping and high power trim states which would be avoided under normal operating conditions, but that level of redundancy still exists, so they are included for the sake of demonstration of the concept.

Response Surface Model Formulation

In a trim procedure, a set of controls equal to the number of trim degrees of freedom are solved such that the forces and moments of the vehicle are within a certain tolerance of zero. Similarly, a set of response "trim variables" (Y) must

Table 2. UH-60A main rotor control and flapping limits

Rotor Condition	Limits
Collective Pitch	$0.4^\circ \leq \theta_{75} \leq 16.4^\circ$
Lateral Pitch	$-8^\circ \leq \theta_{1c} \leq 8^\circ$
Longitudinal Pitch	$-16^\circ \leq \theta_{1s} \leq 16^\circ$
Blade Flapping	$-6^\circ \leq \beta \leq 22^\circ$
Adv. Tip Mach No.	$M_{tip} \leq 0.89$

be chosen, which will be subsequently estimated to approximate trim. The number of controls in Y must be equal to the degrees of freedom in the trim problem (m). For example, an isolated rotor in wind tunnel trim will require three elements in Y, whereas a full helicopter model will require six variables in Y. This ensures that the trim state represented by the variables in Y is unique and fully defined. Any subset of the remaining controls and flight conditions not used in Y will be used as response surface predictors, and contained in X.

For the compound helicopter model in hover, auxiliary thrust and variable main rotor speed provide two degrees of control redundancy, and are selected as the response surface predictors. Consequently, the traditional helicopter trim variables are used for the response variables. This specific set of variables chosen for X and Y is not the only one allowable, and depending on the application it may even be beneficial to interchange elements of X and Y. For this combination of predictors and response variables, X and Y are therefore defined as follows.

$$X = \begin{bmatrix} \Omega & T \end{bmatrix}^T$$
$$Y = \begin{bmatrix} \theta_0 & \theta_{1c} & \theta_{1s} & \delta_T & \alpha & \phi \end{bmatrix}^T$$

Let the function $f_i(X)$ define a response surface that approximates the i^{th} element of Y. For each of the n elements of Y, $f_i(X)$ produces an m dimensional surface in an $m+1$ dimensional space. For any X, a set of controls given by $\hat{Y}$ can be predicted by solving $f_i(X)$ for each element of $\hat{Y}$, from 1 to n. Since the response surface models are trained on control data that satisfy trim, the set of controls in $\hat{Y}$ will approximate the controls needed for an aircraft to be trimmed, subject to the redundant controls and flight conditions given by X. Initially, a quadratic model will be used to produce the response surfaces, with coefficients in A, B, and C, determined through regression analysis to fit a training data set of (X,Y) pairs that are obtained from the RCAS trim sweeps.

$$\hat{Y}_i = f_i(X) = C + BX + X^T AX$$

C is a scalar value, B is a $1 \times n$ array, and A is an upper diagonal matrix of size $n \times n$. The elements of B are the linear coefficients of each predictor, the diagonal elements of A are the square coefficients of each predictor, and the off-diagonal elements are the interaction coefficients between any two predictors.

A regression analysis is performed on the set of trim data for the compound helicopter in hover, which yields the coefficients for a set of quadratic response surfaces that can be used to predict each element of Y as a function of X. The R^2 of each response surface can be used to judge how well the quadratic model captures the data. Figures 1–6 compare the response surfaces plotted as a function of both predictors in X, against the data values that each surface was fit to. The coloring of each data point indicates its vertical distance from the response surface. Each plot includes the adjusted R^2 value, a quantity used to measure quality of fit for the regression, which are also tabulated in the first column of Table 3.

Table 3. Adjusted R^2 of regression models

	Hover	100 kts	100 kts Trunc.
Coll. pitch	0.9974	0.7614	0.9892
Lat. pitch	0.9921	0.6286	0.9977
Long. pitch	0.9949	0.9410	0.9993
Diff. thrust	0.9837	0.6349	0.9956
Pitch attitude	1.0000	0.9981	0.9999
Roll attitude	0.9904	0.4198	0.7585
Total power	1.0000	0.9998	0.9996

The R^2 values for this modeling approach range from 0.98 to 1, with pitch attitude being nearly perfectly predicted, while the differential thrust used to provide counter-torque is the least well-predicted. Of each trim variable, the largest discrepancies occurred at very low RPM. This is likely due to the inboard section of the rotor beginning to stall at low RPM, which will increase necessary blade pitch, blade drag, and consequently the differential propeller pitch setting to overcome the increased torque. The non-linear aerodynamic effects therein will result in the controls behaving less quadratically, for which a quadratic regression model is not able to accurately capture the physics.

Optimization to Find Nearest Approximate Trim State

The set of six response surfaces that have been found for hover describe an infinite number of sets of approximate trim variables, but many of these trim states could be undesirable. An optimization on X can be used to find the set of controls $(X_f, \hat{Y}_f)$ which approximately satisfy trim while minimizing a desired cost function to identify a single set of relevant controls. This optimization can be formulated to satisfy any desired cost function. For instance, simultaneously locating the point on all six surfaces that is closest to the current control states and flight conditions will effectively minimize control effort. Beginning with a set of reference conditions (X_0, Y_0) which may or may not satisfy trim, a control effort minimization routine would be performed on the following cost function.

$$d = \left\| \begin{bmatrix} X \oplus \hat{Y} \end{bmatrix} - \begin{bmatrix} X_0 \oplus Y_0 \end{bmatrix} \right\|_2$$

This process yields X_f, which can then be passed through the response surfaces to give the corresponding $\hat{Y}_f$ controls.

To prevent extrapolation, bounds are set to be equal to the most extreme values that have been sampled in flight (or in

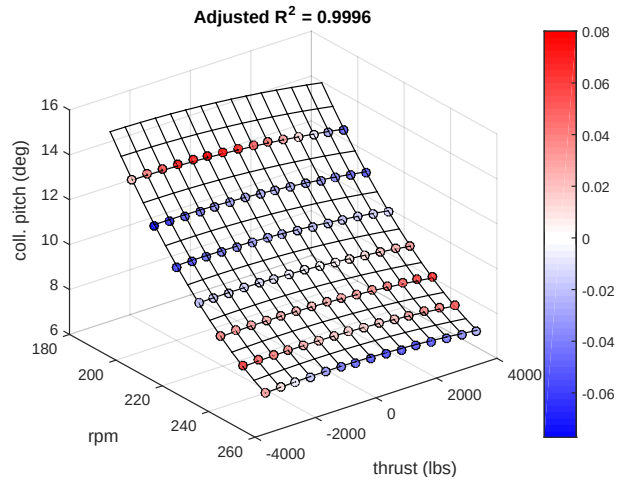

Fig. 1. Collective pitch data vs. response surface model

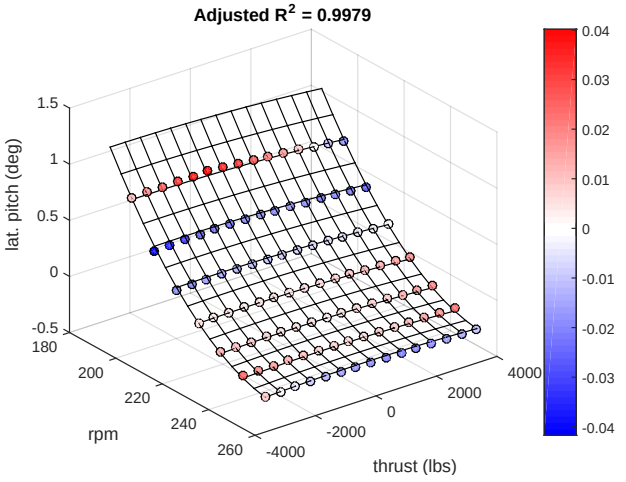

Fig. 2. Lateral pitch data vs. response surface model

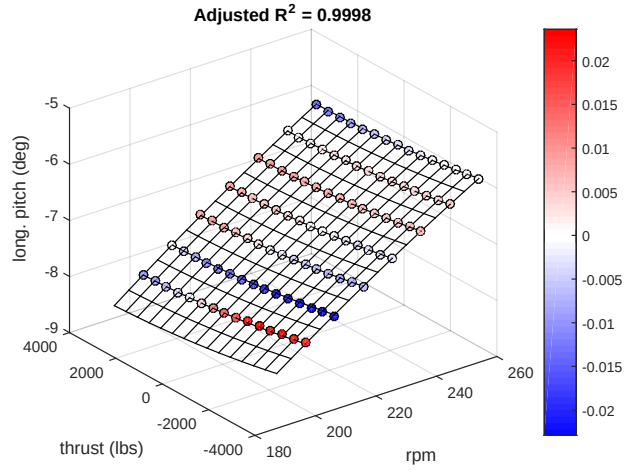

Fig. 3. Longitudinal pitch data vs. response surface model

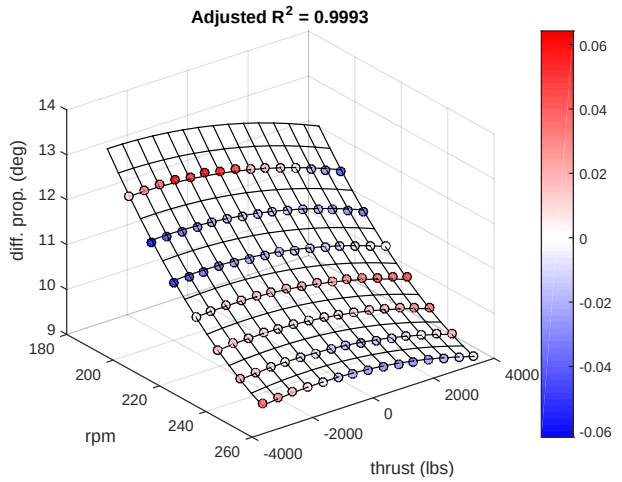

Fig. 4. Diff. prop. pitch data vs. response surface model

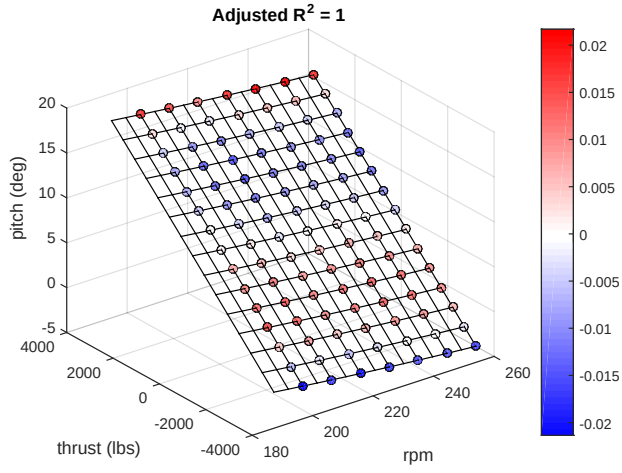

Fig. 5. Pitch attitude data vs. response surface model

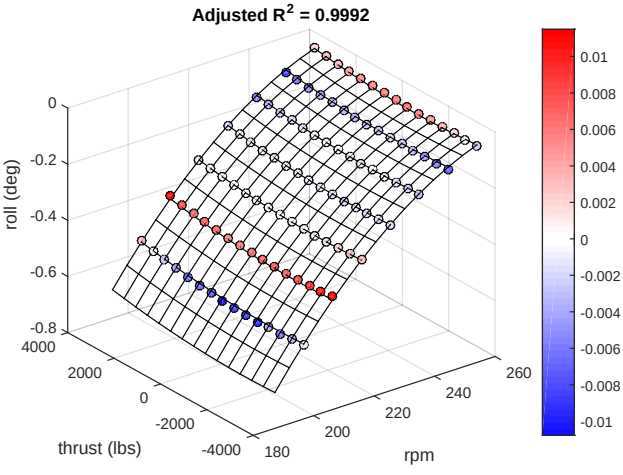

Fig. 6. Roll attitude data vs. response surface model

the simulations). Constraints can be used to limit advancing tip Mach number, or even blade flapping, if an additional response surface were used to model blade flapping. For example,

$$V_\infty + R\Omega \leq 0.9a$$

limits the advancing tip speed to Mach 0.9, which would be a useful constraint in high-speed flight regimes. Additionally, bounds can be used to restrict elements of X from changing. For example, by bounding V_∞ to the desired flight speed both on the upper and lower bound, the provided controls will be in trim without any change to flight speed (if it were being used as a predictor).

RESULTS IN HOVER

By selecting reference conditions (X_0, Y_0) from the simulated data on which the response surfaces have been trained and minimizing the control effort as described previously, a measure of fit that combines all six regression fit models can be produced. Figure 7 plots the 2-norm distance, d, as a function of X, which shows how far each reference condition was from its closest set of approximate trim controls. This figure effectively compiles the total effect of the residuals between the RCAS data and response surfaces which were observed for each of the models in Figures 1–6.

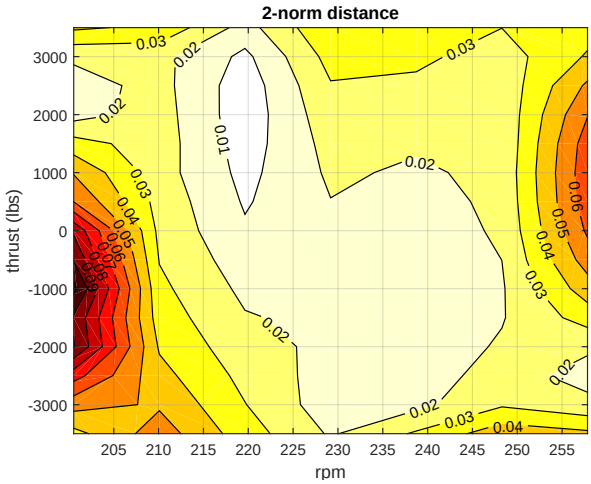

Fig. 7. Trim state data vs. response surface approximated trim after optimization

Since the reference conditions selected are sets of controls which produce actual trim states, any distance between them and the surfaces represents error in the regression fit. The regions of low RPM which corresponded to high error in the regression model also produce the largest total variance in Figure 7. At worst, the total distance is less than 0.1°, while most combinations of rotor speed and auxiliary thrust produce errors of less than 0.03°, demonstrating good agreement between the model and the simulation data.

To determine the true deviation from trim equilibrium, a periodic solution for each set of final approximate trim variables $(X_f, \hat{Y}_f)$ is performed in RCAS, from which the net force and moment data is collected. Figures 8 and 9 show the net residual force and moment for each combination of main rotor speed and auxiliary thrust. The total residual force varies from $20-120$ lbs, while the total residual moment varies from $50-400$ lbs-ft. For comparison, the tolerances used in obtaining trim were 40 lbs of total force and 40 lbs-ft of total moment magnitudes.

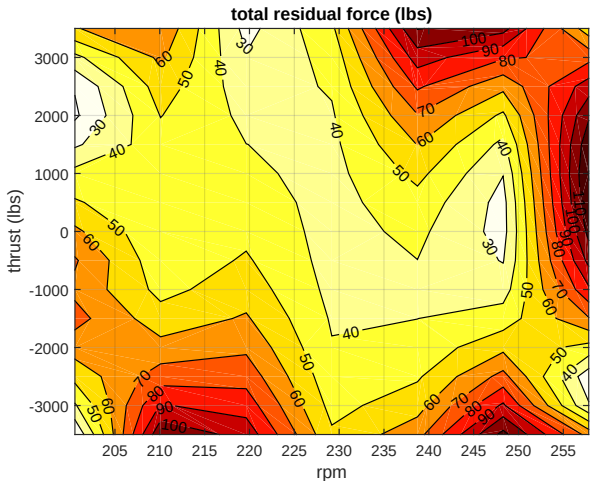

Fig. 8. Residual force magnitude from response surface approximated trim

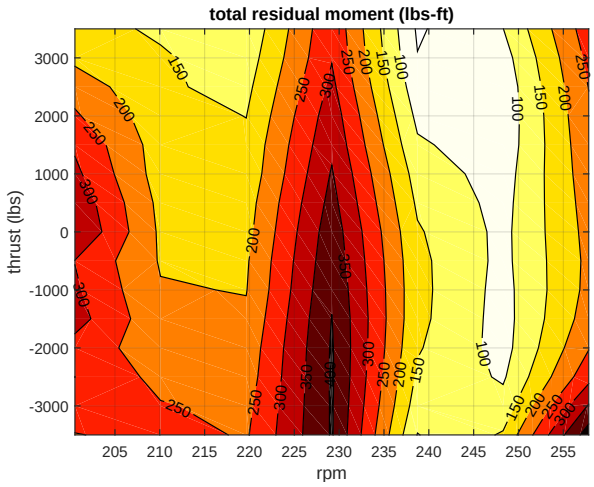

Fig. 9. Residual moment magnitude from response surface approximated trim

RESULTS AT 100 KTS

At forward flight speeds, additional controls such as stabilator and aileron deflection have enough authority to be used as trim controls and consequently, response surface predictors. In this

study, trim states with non-zero aileron deflections were not simulated, so only one additional control (stabilator pitch) is considered. At 100 kts, there are 416 trim states which satisfy the control and flapping limits from Table 2, which are produced by sweeping auxiliary thrust from 0 to 3250 lbs in increments of 500 lbs, rotor rotational speed from 20 to 27 rad/s in increments of 1 rad/s (191 to 258 RPM), and stabilator pitch from $-15°$ to $18°$ in increments of $3°$.

With the addition of a third redundant control, each of the six response surfaces can be considered to be a 3D hypersurface in a 4D space, and cannot be easily represented in a plot as was done for hover in Figures 1–6. Instead, the second column of Table 3 provides the adjusted R^2 values of the aircraft at 100 kts for easy comparison against the corresponding values in hover. At 100 kts, the correlation of the quadratic fit models for collective pitch, lateral pitch, and differential thrust are between 0.62–0.77, with vehicle roll attitude as low as 0.42. In hover, these R^2 values were all greater than 0.98.

Figure 10 compares actual to predicted trim control values by performing leave-one-out comparison tests. For each point on the figure, a model is constructed using each data point except for one. The "left out" data point is then used as reference conditions and a predicted set of trim controls are found by minimizing the 2-norm of the controls between the reference point and the response surfaces (as was done with hover). By comparing the RCAS controls against the predicted controls, trends in error can be observed. For example, Figure 10 shows that there is a pattern in the model of under-prediction at high values of lateral pitch, pedal, and roll attitude. The consistent under-prediction for certain combinations of predictors suggests that there is non-quadratic behavior of the trim variables, which is not being captured by the quadratic response surface model.

Figure 11 shows a slice of constant stabilator, and compares the response surface model to the RCAS simulation values for lateral pitch. The color of the point shows how much error there is between the model and the simulation. Most of the under-prediction of the model can be attributed to the non-quadratic behavior of the controls at values of low RPM and low thrust. Under these conditions, the rotor has high lateral pitch, which is being consistently under-predicted by the values on the response surface. This lack of model fit at low RPM and low thrust is what is responsible for the under-prediction observed in Figure 10 for lateral pitch as well as pedal and roll attitude. During the least squares regression fit, these points skew the quadratic model in such a way that even the controls that follow a quadratic curve are inaccurately captured.

The fit of the model can thus be expected to greatly improve by eliminating the poorly behaved points from the model. In Figure 10, the red data points correspond to all trim state predictions that are greater than 1.5 times the inner quartile range of the error in predicting the RCAS simulation value of the lateral pitch. By eliminating these points from the training, a new model can be obtained which can be expected to have much better correlation between the simulation and the response surface model predicted trim.

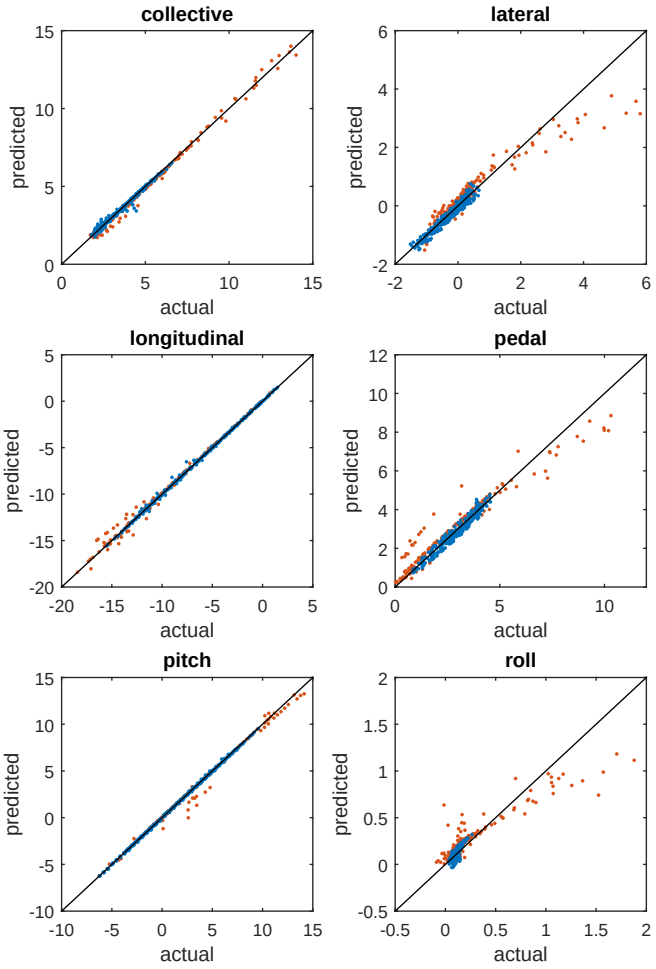

Fig. 10. Comparison of actual to predicted control values on full data set

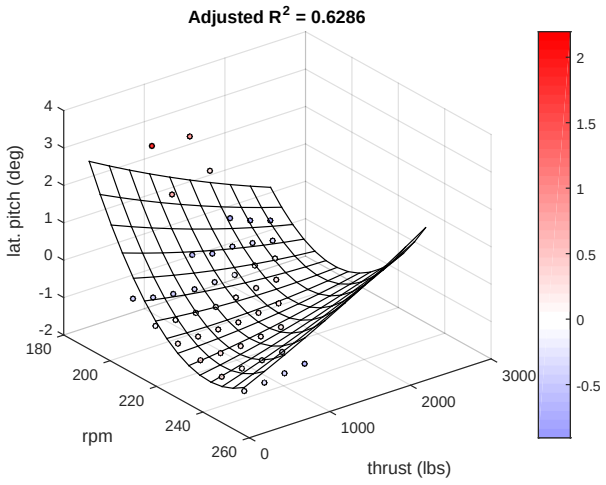

Fig. 11. Lateral pitch data vs. response surface model, all trim states (fixed stab)

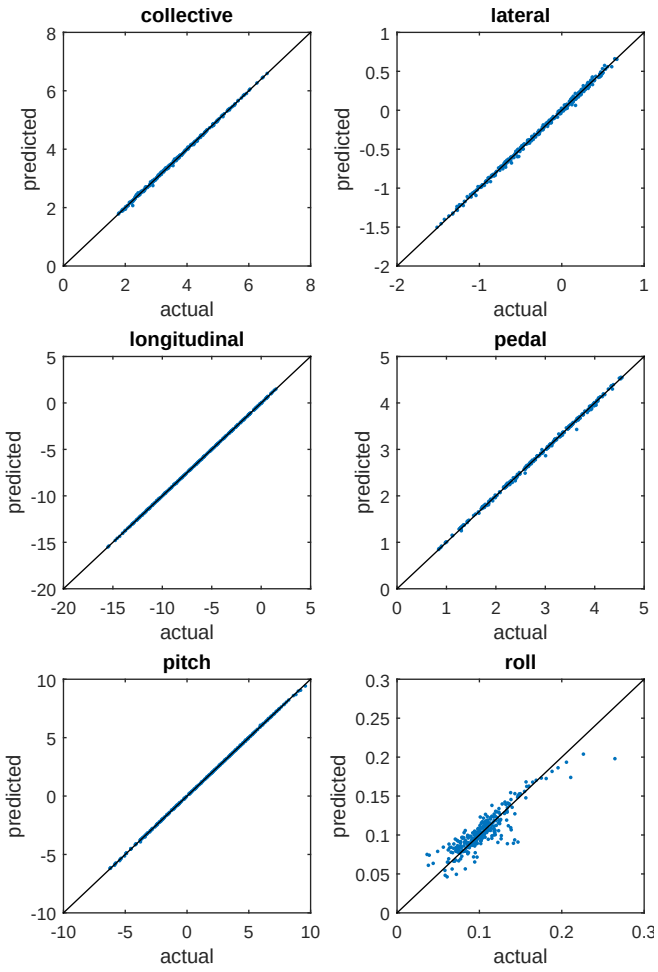

Fig. 12. Comparison of actual to predicted control values after eliminating outlier data

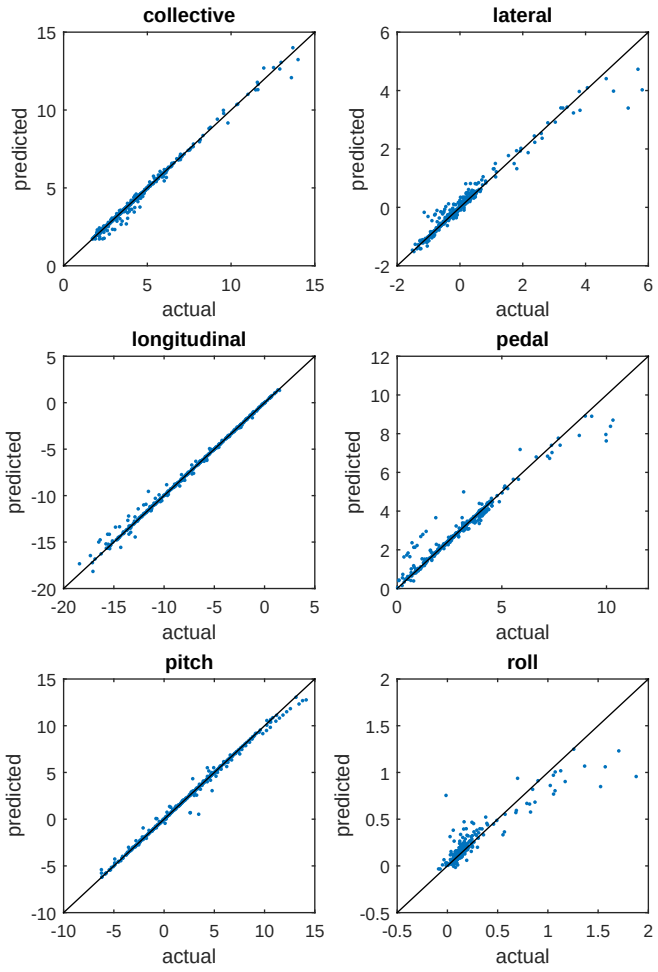

Fig. 14. Comparison of actual to predicted control values using a Kriging model

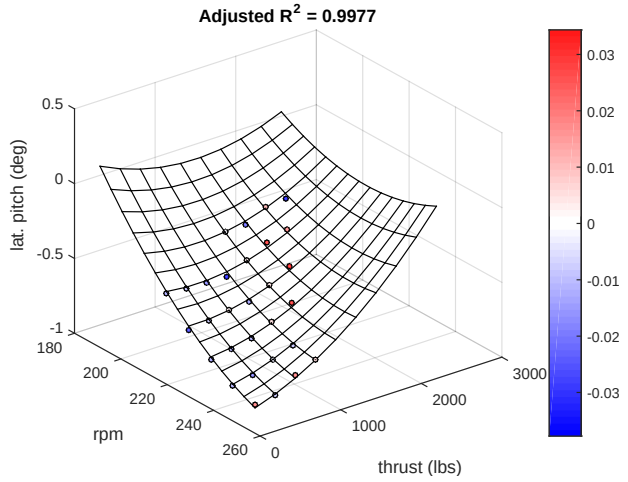

Fig. 13. Lateral pitch data vs. response surface model, truncated set of trim states (fixed stab)

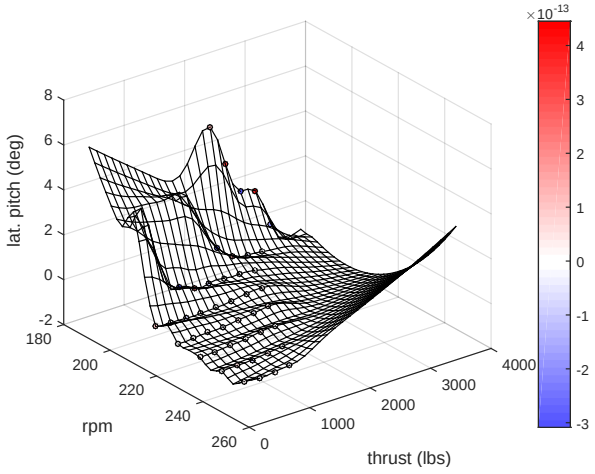

Fig. 15. Lateral pitch data vs. response surface model, Kriging (fixed stab)

Figure 12 shows the new leave-one-out prediction comparative plots. Relative to the full data set of Figure 10, the correlation for all variables is much tighter between the RCAS simulation and the response surface predictions. This is corroborated by the final column of Table 3, which shows the new R^2 for the truncated data set. For each trim variable, the adjusted R^2 is now much closer to 1, with all variables except roll attitude greater than 0.98.

Figure 13 shows the truncated response surface model at the same fixed stabilator pitch as in Figure 11, which highlights the improvement in lateral pitch prediction, but also shows the omission of the large lateral pitches seen at low RPM and low thrust. This issue extends to other controls, and can also be observed by comparing the axes of Figures 10 against 11—where the red points are omitted, the range of applicability of the response surface models of each control is reduced. Since the low thrust and low RPM trim states have been omitted, all of the highest values of collective pitch, lateral pitch, and pedal must be ignored to prevent erroneous extrapolation. For example, collective predictions for the truncated data set are now much more tightly clustered around the line of perfect prediction, but only extend from about $2^\circ - 7^\circ$, which is less than half of the $2^\circ - 14^\circ$ range of the full data set.

Kriging

Kriging is an interpolation approach which correlates errors of a model, and uses it to improve the prediction. The quadratic regression model being used can be expanded to include Kriging interpolation as follows.

$$\hat{Y}_i = f_i(X) + Z(X) = C + BX + X^T AX + Z(X)$$

$Z(X)$ can take a variety of forms, and represents a stochastic process for estimating the deviation in $\hat{Y}$ from the quadratic regression model, $f_i(X)$. The most commonly selected shape of $Z(X)$ for use in surrogate modeling for engineering purposes is a weighted Gaussian function (Refs. 38–40). The Kriging model parameters and weights are determined through DACE (Ref. 41), a free to use MATLAB toolbox.

The resulting response surface is one in which the full range of data can be preserved while maximizing correlation between the actual and predicted values from the model. Figure 14 shows the leave-one-out prediction capabilities of the Kriging response surface model, while Figure 15 shows the same lateral pitch prediction as has been shown for the polynomial regression model and the truncated one. Figure 15 provides a graphical representation of how Kringing is implemented. There is an underlying polynomial surface similar to that of Figure 11, and on top of that are a series of Gaussian regions of influence which produce a deviation from this surface to better fit the RCAS simulation data. With enough resolution of training data to capture the non-quadratic errors through Kriging, the model could provide a very close fit of

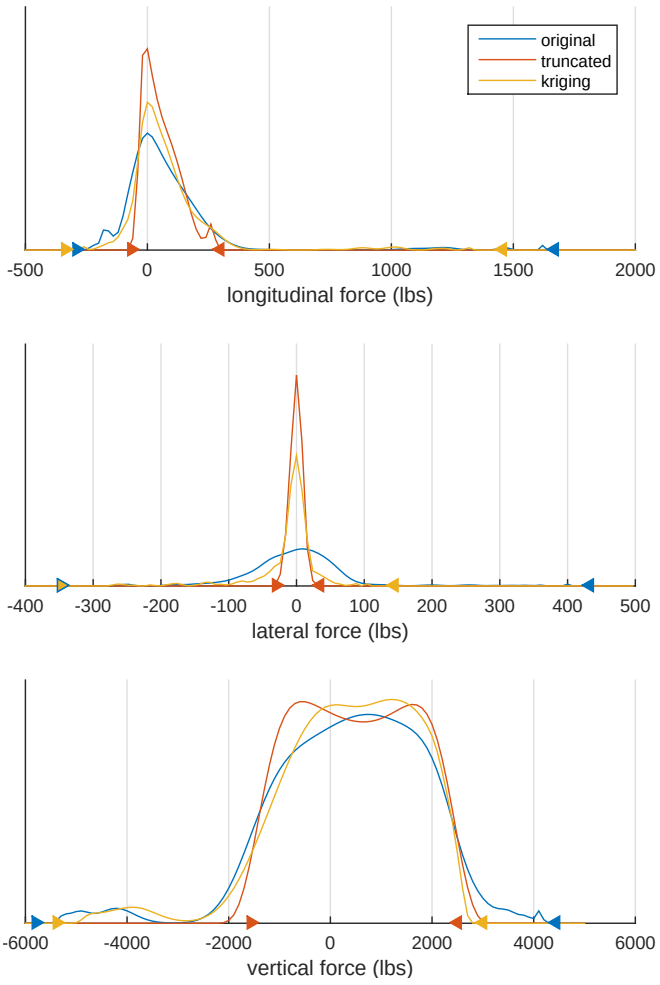

Fig. 16. Residual moments at predicted trim states

the data, but through comparison of the leave-one-out prediction trials, it is clear that even with the sampling density provided, there remains significant error in the response surface. The key benefit of Kriging however, is that the entire range of control actuation in Figure 15 is maintained.

To objectively evaluate the accuracy of the total trim state predictions at 100 kts and compare the three modeling methods described here, periodic solutions are run for leave-one-out predictions after having used each left out RCAS data point as reference conditions. Since the dimensionality of the predictors is too high to represent graphically in two dimensions (as was feasible in Figures 8 and 9, it is presented as density plots for each of the three methods in Figures 16 and 17. These density plots are similar to histograms, but the area under the curves is conserved between each of the three lines, which allows for direct comparison of residual force and moment trends over the control domain, despite being produced with different quantities of periodic solutions depending on the model. By comparing the density curves, the effects of model selection upon force and moment residuals can be easily compared.

In both the longitudinal force and lateral force residuals in Figure 16 it is clear that relative to the original data set, both

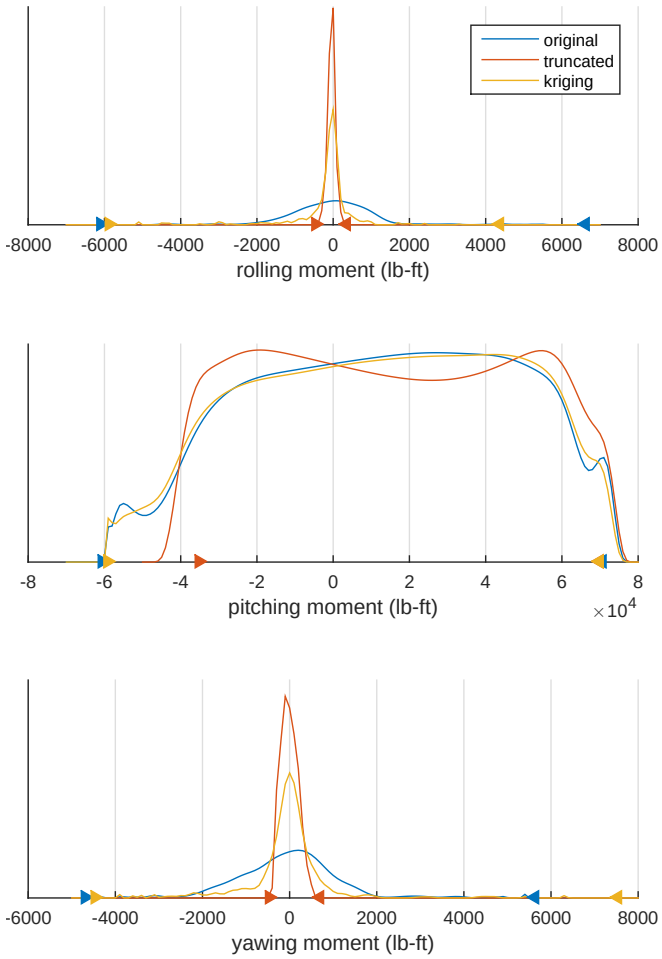

Fig. 17. Residual moments at predicted trim states

Kriging and truncating increase the percentage of states that have near zero force residuals. They also reduce the range of residual force, as indicated by the triangle markers on the x-axis. These markers show the minimum and maximum force of all periodic solutions run, and their values are summarized in Table 4. The truncated data set produces the smallest range of residual force and the greatest density of zero residual force. Kriging both reduces the total range of residual force, and provides an increase in the zero residual force density from the original data set. For vertical force, which is the dominant force direction, the increase in low residual force density for both Kriging and truncated data sets is slight, as are the changes to the maximum force residuals. Truncating the data set reduces the maximum range of the total forces by 59%, and Kriging reduces the maximum range by 8%.

Figure 17 shows the density plot of residual moments for each of the three response surface methods. Similar to lateral and longitudinal force, the rolling and yawing moment residuals are reduced with a Kriging model, and are reduced to an even greater degree by truncating the data set. The pitching moment residuals however, are the dominant moment direction, and demonstrate less significant improvements. It is clear that while improvements to the response surface model can improve force and moment residuals, the benefits are limited in the cases of pitching moments. The improvements to the total pitch moment magnitudes in Table 4 is insignificant.

Figure 18 provides an explanation for the large residuals in the vertical force and pitching moment directions. This figure provides the control sensitivities of each direction plotted against airspeed for hover and 100 kts. The sensitivities presented are the median values of those from the RCAS trim simulations for the six trim variables that were selected as the controls to be predicted by the response surfaces. Of the three force directions, the greatest force responses with change in controls exist in the vertical direction. In the case of moments, the greatest sensitivities exist in the pitching moment. These sensitivities also tend to increase as airspeed does, with more controls acting with higher sensitivity in vertical force and pitching moment. As such, the vertical force and pitch moment directions at 100 kts are the most sensitive to errors in controls. At this speed, one degree of collective pitch error at 100 kts will produce almost 2000 lbs of vertical force, but only 100 lbs of longitudinal force and less than 20 lbs of lateral force. The low sensitivity in each direction to roll attitude also explains why such a low adjusted R^2 for roll attitude correlation can be tolerated without producing large residuals (Table 3).

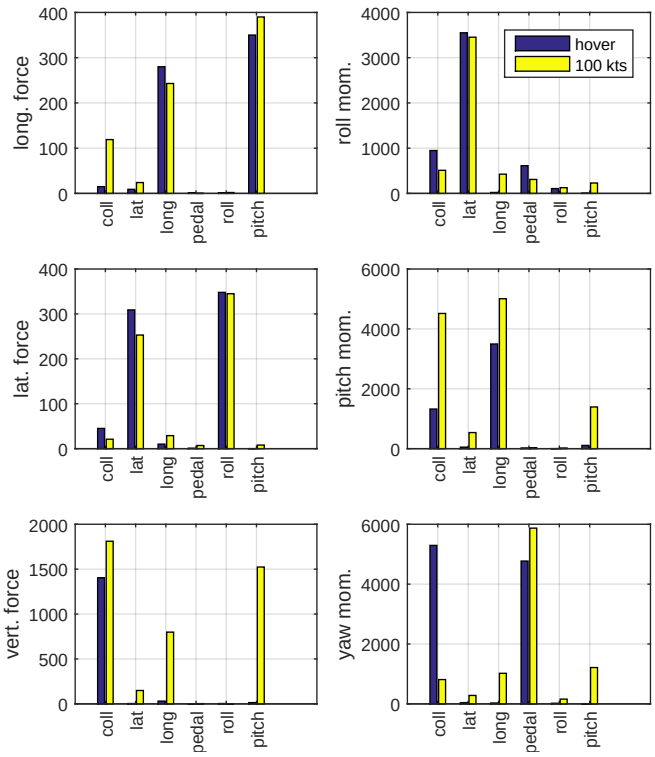

Fig. 18. Control sensitivities in each force and moment direction over three flight speeds (lbs/deg or lbs-ft/deg)

Each of these methods can be used to produce a set of controls which come within a degree of the RCAS obtained controls that were used to train the model, but since the high sensitivities across control axes can result in excessive total

Table 4. 100 kts force and moment residuals for each response surface model

	Original		Truncated		Kriging	
	Min.	Max.	Min.	Max.	Min.	Max.
Longitudinal force (lbs)	−292	1,667	−66	300	−333	1,453
Lateral force (lbs)	−352	432	−30	34	−352	145
Vertical force (lbs)	−5,798	4,432	−1,558	2,493	−5,370	2,996
Roll moment (lbs-ft)	−6,105	6,634	−469	366	−5,889	4,500
Pitch moment (lbs-ft)	−60,630	70,670	−35,330	69,750	−59,290	69,750
Yaw moment (lbs-ft)	−4,692	5,644	−483	694	−4,478	7,540
|Total force| (lbs)	38	6,043	16	2,496	13	5,574
|Total moment| (lbs-ft)	127	70,688	74	69,740	96	69,750

forces and moments, it is clear that the response variables estimated by the response surfaces does not always guarantee trim equilibrium. It is therefore concluded that response surface trim estimation cannot produce a set of trim variables which can be solely relied upon to produce trim, and will still require a feedback controller or equivalent system to maintain trim. The following section describes an application in which response surfaces can still be used to beneficially guide such a trim controller.

MINIMIZATION OF POWER OR ANOTHER DESIRED METRIC

Minimum Power in Hover

The control redundancy in compound helicopters permits an infinite number of trim states to exist. By solving for six of the control variables to maintain trim while allowing the remaining controls to vary, the problem can be recast as an optimization of some target metric, such as total vehicle power. In Refs. 33, 34 a Fly-to-Optimal approach is used in-flight, wherein the additional controls are exercised slowly over time to gradually converge upon the minimum power trim state. As mentioned previously, this approach takes an extended period of time to work, is dependent on the order of controls perturbed, and relies on constant flight conditions throughout the process. The knowledge based solution given by the response surfaces can be used to provide an immediate, albeit approximate setting for the additional controls.

For the analysis in the previous section of this paper, the optimization routine located a trim condition that was closest to a reference condition. The optimization routine can also be used to find the minimum of a desired quantity while satisfying trim. For this optimization scheme, an additional response surface would have to be found (through regression or Kriging) which models the quantity to be minimized. For example, a response surface that predicts power as a function of both X and $\hat{Y}$ could be used to find the approximate controls for a minimum power trim state. In this case the cost function would be as follows.

$$\hat{P} = g(X, \hat{Y})$$

Trim is ensured by optimizing on the variables contained in X, and then solving for $\hat{Y}$ before solving for power.

Figure 19 shows contours of power in hover as calculated by RCAS in the simulations. A quadratic response surface is fit for this data as a function of the two additional controls (thrust and RPM), as well as the six trim controls. Due to the convex nature of the quadratic response surface shape, there is only one global minimum. Therefore, regardless of which trim condition was used, all initial states converge upon the same solution. This point is marked on Figure 19, and is summarized in Table 5 alongside the lowest power case that was obtained through trim sweep in the RCAS analysis. In the second column of Table 5, the values outside of the parentheses are those obtained through power minimization over the response surface model.

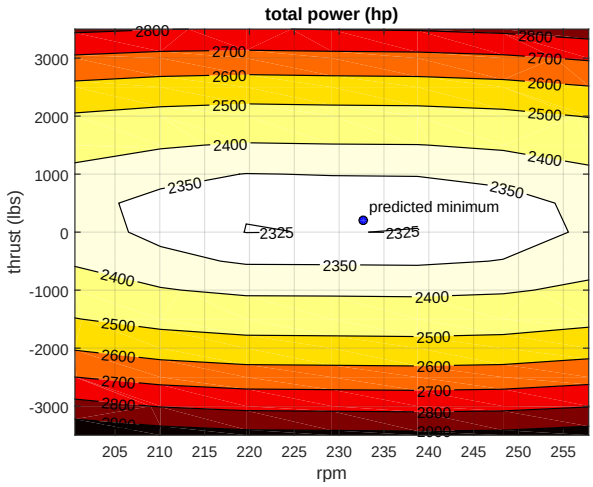

Fig. 19. RCAS simulation of power with predicted minimum power labeled

While the controls and total power estimates generated by the response surfaces are not identical to the state produced in RCAS, they are a very close approximation. The predicted power is within 4 hp, and the two greatest differences in controls are the 0.4° overestimation of the collective pitch required and 227 lbs of collective rotor thrust. It may even be the case that the controls for the true minimum power state lie closer to the response surface prediction, but weren't captured in the trim sweeps due to sampling density.

It is important to note that the estimated controls still pro-

Table 5. Minimum power hover trim states

	RCAS	Quadratic
Coll. pitch	6.9°	7.3° (7.3°)
Lat. pitch	0.5°	0.6° (0.6°)
Long. pitch	−6.1°	−6.2° (−6.2°)
Diff. thrust	2,469 lbs	2,444 lbs (2,483 lbs)
Pitch attitude	6.4°	7.2° (7.2°)
Roll attitude	−0.2°	−0.2° (−0.2°)
Rotor speed	239 RPM	234 RPM
Coll. thrust	0 lbs	230 lbs
Total power	2,325 hp	2,321 hp (2,323 hp)
Residual F_x	0.1 lbs	−30 lbs
Residual F_y	0.2 lbs	−8 lbs
Residual F_z	−2.7 lbs	2 lbs
Residual M_x	1.3 lbs-ft	−28 lbs-ft
Residual M_y	1.3 lbs-ft	159 lbs-ft
Residual M_z	0.3 lbs-ft	290 lbs-ft
Residual F_{tot}	2.7 lbs	31 lbs
Residual M_{tot}	1.9 lbs-ft	332 lbs-ft

duce residual forces and moments, as shown at the bottom of Table 5. Likely related to the overestimation in collective pitch, the estimated controls result in 290 lbs-ft of residual yaw moments. Despite the residual moment, this solution provides a framework through which an aircraft with redundant controls can allocate its additional controls to optimize for power. In the case of the hovering compound helicopter, the pilot or flight controller could control the conventional flight controls, while allowing the response surface to determine the optimal combination of redundant controls (thrust and RPM).

To demonstrate this application, the estimated trim controls were then set as initial conditions for an RCAS trim analysis procedure, which was used to obtain the values in parentheses of Table 5. These controls demonstrate use of the response surfaces to guide trim to a minimum power solution which has an slightly lower power requirement than the lowest power trim state of the training data due to the ability of the response surfaces to interpolate once the model has been produced. All estimated controls match the actual trim controls to within 0.1°, except differential thrust, which is a 39 lbs underestimation of the true value, which addresses the high residual yaw moment reported in the lower portion of the table.

This strategy could also be implemented as a method of determining settings for the additional controls to minimize vibrations, or any other metric for which the aircraft can collect data while in trim. If an even lower power-minimized solution is desired, the response surfaces can provide a knowledge based set of initial conditions from which a Fly-to-Optimal method can be expected to arrive at a minimum power solution more rapidly than with an arbitrary set of initial conditions.

Minimum Power at 100 kts

Relative to the hover approximate trim controls, those which were predicted for flight at 100 kts had larger force and moment residuals. As can be expected, the minimum power states similarly possess a greater degree of control error and residual forces and moments. Table 6 summarizes the controls, power predictions, and the resulting force and moment residuals for the three previously demonstrated methods for comparison against the RCAS data.

The first column of Table 6 shows the controls, power, and residual forces and moments for the lowest power RCAS simulation from the trim sweeps. Each subsequent column presents the response surface estimated trim controls, followed by the RCAS solved true trim controls for the combination of rotor speed, stabilator pitch, and collective thrust for each model.

The estimated minimum power controls determined by the response surfaces from quadratic regression of the full data set are given in the second column. These controls differ by a greater amount than was the case in hover. The estimated total power is 7% lower than the RCAS simulated result, with control estimations differing by even larger amounts. The estimation predicts a lower collective and a higher RPM, as well as only 61% of the propulsive thrust, but only an additional 21% differential thrust for counter-torque. The resulting periodic solution has 1,438 lbs-ft of yaw moment, and generates a net 758 lbs of vertical force. Solving the trim solution yields a substantially different solution than was found in the first column, culminating in a total power which is 12% higher than its prediction.

For most controls, truncating the training data set produces a solution much more similar to the RCAS simulated low power trim state. Only longitudinal cyclic, differential thrust, and vehicle pitch attitude do not improve with the truncated data set, and the total power estimate is now only 2% higher than the RCAS simulated result. The residual forces and moments also benefit, with an 82% reduction in residual force magnitude, and an 86% reduction in residual moment magnitude. The controls predicted by the truncated data set produce an improved prediction both in terms of controls for low power (as compared to the lowest power RCAS simulated case from the trim sweeps), and for controls which are closer to an equilibrium trim state. This is also demonstrated by the parenthetical trim controls and power. Relative to the full data set, there is much less difference between the estimated and solved trim controls. The power prediction was high, but the trim solution produces a minimum power which is slightly lower than was found at any point in the training data, as was the case with hover.

Finally, Kriging is used to optimize for power and compare against the two previously demonstrated response surface methods. Due to the nature of Kriging to introduce localized regions of influence, there exist many non-unique local minima on the total power hyper-surface. This same mechanic can be observed in Figure 15, in which peaks and valleys form in

Table 6. Minimum power 100 kts trim states

	RCAS	Quadratic (all data)	Quadratic (truncated)	Kriging (global min.)	Kriging (local min.)
Coll. pitch	3.4°	2.8° (2.3°)	4.0° (3.8°)	5.3° (5.9°)	3.3° (3.4°)
Lat. pitch	−0.24°	−0.89° (−0.66°)	−0.37° (−0.41°)	−1.5° (−1.1°)	−0.41° (−0.38°)
Long. pitch	−8.2°	−9.0° (−9.7°)	−9.7° (−9.7°)	−16.6° (−17.2°)	−8.8° (−8.9°)
Diff. thrust	414 lbs	503 lbs (618 lbs)	534 lbs (514 lbs)	865 lbs (1,009 lbs)	430 lbs (445 lbs)
Pitch attitude	4.1°	4.3° (4.4°)	4.4° (4.5°)	6.8° (6.9°)	4.5° (4.5°)
Roll attitude	0.10°	0.02° (0.10°)	0.12° (0.11°)	−0.08° (0.04°)	0.09° (0.11°)
Rotor speed	210 RPM	225 RPM	211 RPM	216 RPM	212 RPM
Stab. pitch	0°	−2.8°	−1.6°	−10.9°	−1.3°
Coll. thrust	1,250 lbs	764 lbs	1,014 lbs	0 lbs	1,164 lbs
Total power	783 hp	728 hp (812 hp)	797 hp (781 hp)	761 hp (870 hp)	773 hp (780 hp)
Residual F_x	−1 lbs	−119 lbs	9 lbs	−195 lbs	−28 lbs
Residual F_y	2 lbs	32 lbs	−6 lbs	38 lbs	4 lbs
Residual F_z	23 lbs	758 lbs	−138 lbs	906 lbs	31 lbs
Residual M_x	10 lbs-ft	808 lbs-ft	−81 lbs-ft	1,220 lbs-ft	156 lbs-ft
Residual M_y	34 lbs-ft	729 lbs-ft	231 lbs-ft	842 lbs-ft	323 lbs-ft
Residual M_z	−16 lbs-ft	1,438 lbs-ft	11 lbs-ft	1,625 lbs-ft	345 lbs-ft
Residual F_{tot}	23 lbs	768 lbs	138 lbs	906 lbs	41 lbs
Residual M_{tot}	39 lbs-ft	1,803 lbs-ft	245 lbs-ft	2,199 lbs-ft	498 lbs-ft

regions where the model deviates from the global quadratic regression curve to better fit the data. As a result, a total of eight different minimum power points are found, depending on the initial conditions supplied to the optimizer. Two of these minimum power predictions have been tabulated in Table 6. The first is the global minimum, which predicts the lowest power of all eight, and the second is the most similar local minimum to the RCAS simulated minimum.

The global minimum power found using the Kriging models deviates greatly from all other columns in Table 6. For all controls except main rotor RPM it provides the largest difference from the RCAS simulated minimum. The resulting set of controls also produces the greatest force and moment residuals, which are respectively 18% and 22% larger than those of the full quadratic regression data set, the largest discrepancy between trim control estimates and solved trim controls, and the highest total power corresponding to those trim controls (14% higher than estimated).

While the global minimum of the Kriging model is ill suited to be used as an estimation of the minimum power controls, the Kriging model also is capable of finding a local minimum power solution that performs as good as truncated data set in predicting most controls. The residuals are also comparable to those of the truncated data set. Relative to the quadratic model generated from the full data set, the total residual force of the best Kriging local minima are reduced by 95%, while the total residual moments are reduced by 72%. Using this estimation to allocate the additional controls to reproduce a true trim state in RCAS also yields the lowest power trim state of any model at 100 kts, a slight (¡1%) improvement upon the truncated data set model.

FUTURE WORK

This study was performed using a comprehensive set of training data at each of the two flight speeds for constant density and gross weight. While it was demonstrated that under these ideal conditions, the models could accurately estimate the minimum power trim state, future work will be done to test a more representative set of training data that would be acquired from practical flights. For this set of training data, the response surface predictors will be expanded to include flight conditions such as velocity, density, and gross weight, whereby the response surfaces will be used to predict minimum power at intermediary flight conditions for which there may not exist any model training data.

CONCLUSIONS

1. This paper presents an application of response surface models (typically used in design optimization) to predict the set of controls required to maintain trim as a function of additional controls, and flight conditions. A set of six response surfaces are produced, which predict the six conventional trim controls as a function of the additional controls present on compound helicopters. The models are trained on data produced through RCAS trim analysis while parametrically varying the additional controls.

2. It is found that a quadratic regression fit model performs well in hover to model the response of controls required to maintain trim. At 100 kts, combinations of low thrust and low RPM produces non-quadratic behavior that results in inaccurate response surface models. Two approaches to improving the models are explored. First, eliminating the data that does not follow the quadratic model gives the greatest improvement to the predictive capabilities of the model, but at the cost of a reduced range of applicability for the model. Alternatively, a

Kriging interpolation based response surface will allow the full range of controls, but at the cost of reduced improvements to the predictive accuracy of the model. Even with these improvements, the response surfaces cannot be solely relied upon to guarantee trim.

3. An additional response surface can be produced to track the behavior of an objective metric (such as power) subject to changes in the set of all controls and flight conditions. Through minimization of the power response surface, a set of controls can be given which approximate the minimum power trim state. It is shown that to minimize power, the response surface models produced through the truncated data set produce the best estimate of the RCAS simulated minimum power trim state.The Kriging model produces multiple local minima, one of which does as well as the truncated data set response surface in predicting low power, while the remaining minima (including the global minimum) actually produce trim states with up to 14% higher power.

4. This knowledge guided approach can be used to allocate redundant controls such that a good approximation of the minimum power trim state is produced through using the remaining six trim variables to maintain steady level flight. A Fly-to-Optimal method may also be able to take advantage of response surfaces to produce reasonable initial conditions to improve the speed of the optimization.

Author contact: Jean-Paul Reddinger, reddij2@rpi.edu; Farhan Gandhi, fgandhi@rpi.edu

ACKNOWLEDGMENTS

This research was funded by the U.S. Government under Agreement No. W911W6-11-2-0011. The U.S Government is authorized to reproduce and distribute reprints notwithstanding any copyright notation thereon. The views and conclusions contained in this document are those of the authors and should not be interpreted as representing the official policies, either expressed or implied, of the U.S. Government.

REFERENCES

[1]Leishman, J. G., *The Helicopter—Thinking Forward, Looking Back*, College Park Press, College Park, MD, 2007.

[2]Ruddell, A., "Advancing Blade Concept (ABC) Technology Demonstrator," U. S. Army Research and Technology Labotratories (AVRADCOM), USAAVRADCOM-TR-81-D-5, Apr. 1981.

[3]Bagai, A., "Aerodynamic Design of the X2 Technology^{TM} Demonstrator Main Rotor Blade," American Helicopter Society 64th Annual Forum, Montréal, QC, Canada, Apr. 29–May 1, 2008.

[4]Blackwell, R., and Millott, T., "Dynamics Design Characteristics of the Sikorsky X2 Technology^{TM} Demonstrator Aircraft," American Helicopter Society 64th Annual Forum, Montréal, QC, Canada, Apr. 29–May 1, 2008.

[5]Walsh, D., Weiner, S., Arifian, K., Bagai, A., Lawrence, T., and Blackwell, R., "Development Testing of the X2 Technology^{TM} Demonstrator," American Helicopter Society 65th Annual Forum, Grapevine, TX, May 27–29, 2009.

[6]Walsh, D., Weiner, S., Arifian, K., Lawrence, T., Wilson, M., Millott, T., and Blackwell, R., "High Airspeed Testing of the Sikorsky X2 Technology^{TM} Demonstrator," American Helicopter Society 67th Annual Forum, Virginia Beach, VA, May 3–5 2011.

[7]Colucci, F., "No Single Decision." *Vertiflite*, Nov./Dec. 2014: 10–11.

[8]Hirschberg, M., "Raider Rolls Out." *Vertiflite*, Nov./Dec. 2014: 12–13.

[9]Prouty, R. W., and Yackle, A. R., "The Lockheed AH-56 Cheyenne—Lessons Learned," AIAA-92-4278, AIAA Aircraft Design Systems Meeting, Hilton Head, SC, Aug. 24–26, 1992.

[10]Johnson, W., Yeo, H., and Acree, C. W., "Performance of Advanced Heavy-Lift, High-Speed Rotorcraft Configurations," AHS International Forum on Multidisciplinary Technology, Seoul, Korea, Oct. 15–17, 2007.

[11]Colucci, F., "SpeedHawk—Phase I." *Vertiflite*, Winter 2007.

[12]Nelms, D., "Aviation Week Flies Eurocopters X^3" *Aviation Week & Space Technology*, Vol. 174, No. 24, Jul. 9, 2012.

[13]Balmford, D. E. H., and Benger, B. S., "The Compound Helicopter—A Concept Revisited," 17th European Rotorcraft Forum, Berlin, Germany, Sept. 1991.

[14]Humpherson, D. V., "Compound Interest—A Dividend for the Future, Revised," American Helicopter Society 54th Annual Forum, Washington DC, May 2022, 1998.

[15]Orchard, M. N., and Newman, S. J., "The Compound Helicopter Versus Tilt Rotor—Europes Shortcut to the Future," 26th European Rotorcraft Forum, The Hague, Netherlands, Sept. 2000.

[16]Yeo, H., and Johnson, W. "Optimum Design of a Compound Helicopter," Presented at the Heli Japan 2006 AHS International Meeting on Advanced Rotorcraft Technology and Life Saving Activities, Nagoya, Japan, Nov. 2006.

[17]Yeo, H., and Johnson, W., "Aeromechanics Analysis of a Heavy Lift Slowed-Rotor Compound Helicopter," *Journal of Aircraft,* Vol. 44, (2), Mar./Apr. 2007, pp. 501–508.
doi: 10.2514/1.23905

[18]Floros, M. W., and Johnson, W., "Performance Analysis of the Slowed-Rotor Compound Helicopter Configuration," Vol. 54, (2), Apr. 2009, pp. 1–12.
doi: 10.4050/JAHS.54.022002

[19]Ormiston, R. A., "Low-Disk Loading Compound Rotorcraft for High Speed and Aerodynamic Efficiency," AHS, AIAA, SAE, RAeS International Powered Lift Conference Proceedings, Philadelphia, PA, Oct. 5–7, 2010.

[20]Hall, K. C., and Hall, S. R., "A Variational Method for Computing the Optimal Aerodynamic Performance of Conventional and Compound Helicopters," Vol. 55, (4), Oct. 2010, pp. 1–16.
doi: 10.4050/JAHS.55.042006

[21]Moodie, A., and Yeo, H., "Design of a Cruise Efficient Compound Helicopter," American Helicopter Society 67^{th} Annual Forum, Virginia Beach, VA, May 3–5, 2011.

[22]Moodie, A. M., and Yeo, H., "Design of a Cruise-Efficient Compound Helicopter," *Journal of the American Helicopter Society,* Vol. 57, (3), Jul. 2012, pp. 1–11.
doi: 10.4050/JAHS.57.032004

[23]Rand, O., and Khromov, V., "Compound Helicopter: Insight and Optimization," *Journal of the American Helicopter Society,* Vol. 60, (1), Jan. 2015, pp. 1–12.
doi: 10.4050/JAHS.60.012001

[24]Datta, A., Yeo, H., and Norman, T. R., "Experimental Investigation and Fundamental Understanding of a Full-Scale Slowed Rotor at High Advance Ratios," *Journal of the American Helicopter Society,* Vol. 58, (2), Apr. 2013, pp. 1–12.
doi: 10.4050/JAHS.58.022004

[25]Sekula, M. K., and Gandhi, F., "Effects of Auxiliary Lift and Propulsion on Helicopter Vibration Reduction and Trim," *Journal of Aircraft,* Vol. 41, (3), May–Jun. 2004, pp. 645–656.

[26]Gandhi, F., and Sekula, M. K., "Helicopter Vibration Reduction using Fixed-System Auxiliary Moments," *AIAA Journal,* Vol. 42, (3), Mar. 2004, pp. 501–512.

[27]Sekula, M. K., and Gandhi, F., "Helicopter Vibration and Rotor Power Reduction through Horizontal Tail Incidence Angle Control," American Helicopter Society 60^{th} Annual Forum, Baltimore, MD, Jun. 7–10, 2004.

[28]Gandhi, F., and Sekula, M. K., "Helicopter Horizontal Tail Incidence Control to Reduce Rotor Cyclic Pitch and Blade Flapping," American Helicopter Society 60^{th} Annual Forum, Baltimore, MD, Jun. 7–10, 2004.

[29]Reddinger, J. P., and Gandhi, F., "Performance and Hub Vibrations of an Articulated Slowed-Rotor Compound Helicopter at High Speeds," American Helicopter Society 71^{st} Annual Forum, Virginia Beach, VA, May 5–7, 2015.

[30]Reddinger, J. P., and Gandhi, F., "Physics-Based Trim Optimization of an Articulated Slowed-Rotor Compound Helicopter in High-Speed Flight," *Journal of Aircraft,* Vol. 52, No. 6 (2015), pp. 1756–1766.
doi: 10.2514/1.C032939

[31]Barron, H. M., Brentner, K, Horn, J. F., Ozdemir, G. T., and Thorsen, A. T., "Acoustic Analysis of Compound Helicopters with Trim Variations," American Helicopter Society 69^{th} Annual Forum, Phoenix, AZ, May 21–23, 2013.

[32]Thorsen, A., Horn, J. F., and Ozdemir, G. T., "Use of Redundant Controls to Enhance Transient Response and Handling Qualities of a Compound Rotorcraft," American Helicopter Society 70^{th} Annual Forum, Montréal, QC, Canada, May 21–23, 2014.

[33]Ozdemir, G. T., Horn, J. F., and Thorsen, A., "In-Flight Multi-Variable Optimization of Redundant Controls on a Compound Rotorcraft," AIAA Guidance, Navigation, and Control Conference, Boston, MA, August 19–22, 2013.

[34]Ozdemir, G. T., and Horn, J. F., "Simulation Analysis of a Flight Control Law with In-Flight Performance Optimization," American Helicopter Society 68^{th} Annual Forum, Fort Worth, TX, May 1–3, 2012.

[35]Yeo, H., Bousman, W. G., and Johnson, W., "Performance Analysis of a Utility Helicopter with Standard and Advanced Rotors," *Journal of the American Helicopter Society,* Vol. 49, (3), Jul. 2004, pp. 250–270.
doi: 10.4050/JAHS.49.250

[36]Saberai, H., Khoshlahjeh, M., Ormiston, R., and Rutkowski, M. "Overview of RCAS and Application to Advanced Rotorcraft Problems," AHS 4^{th} Decennial Specialists' Conference on Aeromechanics, San Francisco, CA, Jan. 21–23, 2004.

[37]Jain, R., Yeo, H., Ho, J. C., and Bhagwat, M. "An Assessment of RCAS Performance Prediction for Conventional and Advanced Rotor Configurations," American Helicopter Society 70^{th} Annual Forum, Montréal, QC, Canada, May 21–23, 2014.

[38]Glaz, B., Goel, T., Liu, L., Friedmann, P. P., and Haftka, R. T., "Multiple-Surrogate Approach to Helicopter Rotor Blade Vibration Reduction," *AIAA Journal*, Vol. 47, No. 1 (2009), pp. 271–282.
doi: 10.2514/1.40291

[39]Glaz, B., Friedmann, P. P., Liu, L., Cajigas, J. G., Bain, J., and Sankar, L. N., "Reduced-Order Dynamic Stall Modeling with Swept Flow Effects Using a Surrogate-Based Recurrence Framework," *AIAA Journal*, Vol. 51, No. 4 (2013), pp. 910–921.
doi: 10.2514/1.J051817

[40]Gogulapati, A., Friedmann, P. P., and Martins, J. R. R. A., "Optimization of Flexible Flapping-Wing Kinematics in Hover," *AIAA Journal*, Vol. 52, No. 10 (2014), pp. 2342–2354.
doi: 10.2514/1.J053083

[41]Lophaven, S. N., Nielsen, H. B., and Søndergaard, J., "A Matlab Kriging Toolbox, Version 2.0," Informatics and Mathematical Modeling, Technical Univ. of Denmark, TR IMM-TR-2002-12, Lyngby, Denmark, 2002.